Coordination of Nucleotides to Metals at the M2 and M3 Metal-Binding Sites of Spinach Chloroplast F_1-ATPase†

Andrew L. P. Houseman, Russell LoBrutto, and Wayne D. Frasch*

The Center for the Study of Early Events in Photosynthesis, Department of Botany, Arizona State University, Tempe, Arizona 85287-1601

Received March 28, 1994; Revised Manuscript Received June 9, 1994®

ABSTRACT: Vanadyl (V^{IV}=O)$^{2+}$ was used as a paramagnetic probe at the M2 and M3 metal-binding sites of the spinach chloroplast F_1-ATPase (CF_1) in order to detect interaction of the metals with nucleotides. The M2 site can exist in two forms in the presence of ATP. When ATP and VO^{2+} are added in a 1.5:1 ratio to CF_1, the VO^{2+} EPR spectrum is identical to that of CF_1-VO^{2+} in the absence of ATP. When the M2 site is filled by the addition of ATP and VO^{2+} in a 3:1 ratio, the VO^{2+} binds to M2 in a second form with equatorial coordination to a single phosphate. The treatments required to deplete CF_1 of the monodentate VO^{2+}–nucleotide complex indicate that the VO^{2+} is coordinated to the ATP at the noncatalytic N2 site. The presence of uncomplexed nucleotide appears to induce formation of the second form, possibly via ATP binding to the N3 site. This change in coordination at the M2 noncatalytic site may regulate the ATPase activity of CF_1. The M3 site also exists in two forms: (i) in latent CF_1, no phosphate coordination is evident; and (ii) after the ATPase has been activated, the EPR line shape is consistent with the two phosphates from ADP at N3 coordinated to the VO^{2+} at M3. This work establishes a connection between the metal- and nucleotide-binding sites as M2–N2 and M3–N3.

The chloroplast F_1F_o-ATP synthase uses a transmembrane proton gradient as a source of energy to synthesize ATP from ADP and phosphate on the F_1 portion of the enzyme. When the proton gradient dissipates, the ATPase reaction is prevented by regulatory mechanisms that convert the enzyme from an active to a latent form. The ATPase activity of purified F_1-ATPase from spinach chloroplasts (CF_1)[1] is latent but can be activated by dithiothreitol or ethanol, which either reduces a disulfide on the γ subunit or dissociates the ϵ subunit, respectively [cf. Frasch (1994) for a review].

CF_1 has been estimated to have six binding sites for divalent metal cations (Hiller & Carmeli, 1985). Initial characterization of metal binding to CF_1 has identified three sites, M1–M3, that can be separated due to their unique binding properties. The M1 metal-binding site is the only site that can resist depletion of Mg^{2+} by a 50+ h incubation of the protein as an ammonium sulfate precipitate in the presence of EDTA (Houseman et al., 1994). Latent CF_1 depleted of bound metals and nucleotides by this treatment will bind divalent cations to the M2 and M3 sites in a cooperative manner (Haddy et al., 1985; Hiller & Carmeli, 1985; Houseman et al., 1994).

The bound metals facilitate catalysis in the CF_1-ATPase by coordinating the phosphate oxygens of the nucleotides bound to the catalytic sites (Frasch & Selman, 1982; Carmeli et al., 1986) as well as by binding at noncatalytic sites (Murataliev, 1992; Jault & Allison, 1993). Of the six nucleotide-binding sites estimated to exist on CF_1, five can also be identified by unique binding properties. The ADP at the catalytic N1 site, like the metal at the M1 site, is the only nucleotide that can survive ammonium sulfate precipitation with EDTA for 50+ h followed by gel filtration (Bruist & Hammes, 1981). The noncatalytic N2 site is specific for ATP, nucleotide binding is dependent on Mg^{2+}, and depletion of this site requires the extended ammonium sulfate precipitation and gel filtration treatment. The catalytic N3 site binds ADP with higher affinity than ATP and can be distinguished from the catalytic N4 site using gel filtration chromatography (Bruist & Hammes, 1981; Leckband & Hammes, 1987; Shapiro et al., 1991). The noncatalytic N5 site can be observed using Mg^{2+} ATP (Shapiro et al., 1991).

At least three of the metal-binding sites are associated with the catalytic sites since the nucleotides at the three catalytic sites coordinate the metals to facilitate catalysis. Several indirect observations suggest that the first three M sites are each associated with the first three N sites. Both the M1 and N1 sites remain filled after depletion by ammonium sulfate precipitation, and the N3 site may not have a strict metal dependence perhaps because metal binding to the M2 and M3 sites is cooperative (Houseman et al., 1994; Bruist & Hammes, 1981). However, direct evidence of the interaction between any of the M sites with a specific N site is lacking.

We recently showed that VO^{2+} can serve as a functional metal cofactor for the ATPase reaction catalyzed by CF_1 both at the catalytic sites and at the noncatalytic N2 site (Houseman et al., 1994). We now present a characterization of the changes in the EPR spectrum that occur upon the addition of nucleotides. Little difference is observed when

† This work was supported by U.S. Department of Agriculture NRIC Grant 92-01249 and by Grant 0188HF from the H. Frasch Foundation to W.D.F. This is publication No. 204 of the Center for the Study of Early Events in Photosynthesis. The Center is supported by the U.S. Department of Energy Grant DE-FG02-88ER13969. A.L.P.H. is an ASU Center for the Study of Early Events in Photosynthesis Postdoctoral Research Fellow.

* Author to whom correspondence should be addressed. E-mail address: atwdf@asuvm.inre.asu.edu.

® Abstract published in *Advance ACS Abstracts,* July 15, 1994.

[1] Abbreviations: AdoMet, *S*-adenosylmethionine; CF_1, soluble chloroplast F_1-ATPase; CW-EPR, continuous wave electron paramagnetic resonance spectroscopy; HEPES, *N*-(2-hydroxyethyl)piperazine-*N*′-2-ethanesulfonic acid; M1, the metal-binding site with highest affinity; M2 and M3, cooperatively binding high-affnity metal sites; N1, nondissociable catalytic nucleotide-binding site; N2, metal-dependent ATP-specific nucleotide site dissociable only upon precipitation in $(NH_4)_2SO_4$ and EDTA; N3; most tightly bound ADP-specific dissociable catalytic site; P_i, inorganic phosphate; PPP_i, tripolyphosphate.

0006-2960/94/0433-10000$04.50/0

VO^{2+} fills the M2 site in the presence of ATP unless the ATP concentration approaches twice the metal concentration. Under these conditions, if the M1 site contains Mg^{2+}, CF_1 binds the VO^{2+}–ATP as a monodentate complex. This is the first direct evidence that correlates the M2 and N2 sites. Activation of the enzyme changes the EPR spectrum of the VO^{2+}–ADP bound to the M3 site. This change and an apparent ^{31}P hyperfine splitting are consistent with the coordination of multiple nucleotide phosphate oxygens, suggesting a correlation between this site and the catalytic N3 site.

EXPERIMENTAL PROCEDURES

Protein Purification and Sample Preparation. CF_1 was isolated as described previously (Houseman et al., 1994). Metal and nucleotide depletion procedures were the same as those reported by Houseman et al. (1994) and Bruist and Hammes (1981), respectively. Solutions of VO^{2+} were prepared fresh daily using water that had been thoroughly sparged with dry $N_2(g)$ to remove dissolved O_2. Some samples of CF_1 were activated in 50 mM DTT and 20% ethanol after VO^{2+}–ATP or VO^{2+}–ADP had been added to the latent form.

ATP Binding with [2,8-^{3}H]ATP. To determine whether the ATP:VO^{2+} ratio had an effect on the binding of ATP at N2, binding studies were conducted with [2,8-^{3}H]ATP. [2,8-^{3}H]ATP and either VO^{2+} or Mg^{2+} were added to CF_1 in a 1.5:1:1 ratio and a 3:1:1 ratio with CF_1 at 0.11 mg/mL. The mixture was then chromatographed on a 30-cm column of Sephadex G-50-80 equilibrated in 50 mM HEPES buffer at pH 8.0 in order to remove all nucleotide in sites N3–N6 and all metal in sites M3–M6. The number of equivalents of [2,8-^{3}H]ATP left bound to the protein at the N2 site was then measured by liquid scintillation counting.

EPR Measurements. CW-EPR experiments were carried out at X-band (9 GHz) using a Bruker 300E spectrometer and a liquid nitrogen flow cryostat operating at 100K as described previously (Houseman et al., 1994).

Determination of Relative Abundance of Species. The abundance of protein-bound VO^{2+} species was determined by the areas of the EPR signals at the $-5/2_{\|}$ position as per Houseman et al. (1994). When two or more species had overlapping signals, their contributions to the total area were found by use of the program SpectraCalc for the IBM PC. Given the number of Gaussian or Lorentzian peaks in a spectrum and an initial estimate of their positions, heights, and full-widths at half-heights, this program finds a best fit of the spectrum and gives the areas corresponding to each component. SpectraCalc was also used to select a baseline through the data in the $-5/2_{\|}$ region.

Atomic Absorption Spectroscopy and Correlation of EPR Signal Intensities and VO^{2+} Concentration. VO^{2+}–ATP was added to metal–nucleotide-depleted CF_1, which was then chromatographed on a Sephadex G-50-80 column to remove all VO^{2+} not tightly bound. The $-5/2_{\|}$ EPR signal of bound VO^{2+} was integrated and correlated to the abundance of vanadium by atomic absorption spectroscopy as described earlier (Houseman et al., 1994).

Resolution Enhancement. Enhancement of spectral resolution in CW-EPR spectra was accomplished by the Fourier self-deconvolution method of Kauppinen et al. (1981), as adapted for EPR by Latwesen et al. (1992). The spectrum was Fourier transformed, deconvoluted from a Lorentzian function (by multiplication by $\exp(2\pi\sigma|t|)$, where σ is the line width), then apodized using the window function $(1-|x|/L)^2$ (where L is entered as a parameter), and inverse Fourier transformed. A more detailed description of the procedure is given by Latwesen et al. (1992). The resolution-enhancement software employed for this study is a local C-language adaptation of an original FORTRAN program, which was a generous gift of Dr. G. H. Reed.

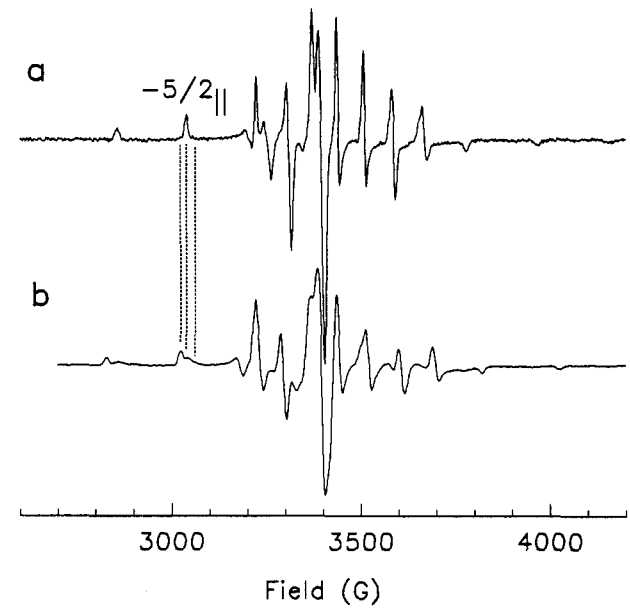

FIGURE 1: CF_1 depleted of metal and nucleotide in the presence of (a) 1.5 ATP per VO^{2+} and (b) 3 ATP per VO^{2+}. Experimental spectra taken at 100 K, 9.55 GHz, 5 G modulation amplitude, 9.52 G/s sweep rate (SR), and 100 kHz modulation frequency. Other conditions: (a) 1 mW microwave power; 82 ms time constant (TC); 4 scans; 2.0 equiv of VO^{2+} were added to 43.6 mg of CF_1 at a total volume of 465 μL; (b) 2.5 mW microwave power; 9.5563 GHz; TC, 328 ms; 2 scans; 0.67 equiv of VO^{2+} was added to 153 mg of CF_1 at a total volume of 255 μL.

RESULTS

Metal Binding in the Presence of Nucleotide. The addition of a 1.5:1 mole ratio of ATP:VO^{2+} to latent CF_1 that had been depleted of metals and nucleotides by incubation as a precipitate in ammonium sulfate for 50+ h results in the EPR spectrum of VO^{2+} bound to CF_1 shown in Figure 1a. This spectrum contains the 16 lines characteristic of a single average ligand environment of VO^{2+} with an axial ^{51}V hyperfine coupling tensor (Chasteen, 1981). The binding of VO^{2+} in the absence of nucleotide to the protein prepared in the same manner results in an EPR spectrum which is virtually identical to that of Figure 1a (Houseman et al., 1994). In the absence of nucleotide, Mn^{2+} or VO^{2+} binds in a cooperative manner to the M2 and M3 sites (Haddy et al., 1985; Houseman et al., 1994). The ^{51}V hyperfine coupling is very sensitive to the types of groups that comprise the equatorial ligands (Chasteen, 1981). However, because the ^{51}V hyperfine coupling represents the weighted average of the number of each type of ligand in a mixed ligand environment, more than one group of ligands may give rise to very similar CW-EPR spectra. Thus, it is possible that the M2 and M3 sites are distinct sites with different equatorial ligands.

The EPR spectrum of VO^{2+} that bound to CF_1 upon the addition of a 3:1 ATP:VO^{2+} mole ratio is more complex (Figure 1b). This spectrum contains the 16-line spectrum of Figure 1a, but two additional 16-line spectra are also apparent. The individual components that compose Figure 1 are most readily distinguished in the $-5/2_{\|}$ region of the spectrum, which is shown in greater detail in Figure 2. When VO^{2+} has bound to CF_1 under conditions in which free VO^{2+} is limiting but ATP is in excess, the most prominent new feature in the $-5/2_{\|}$

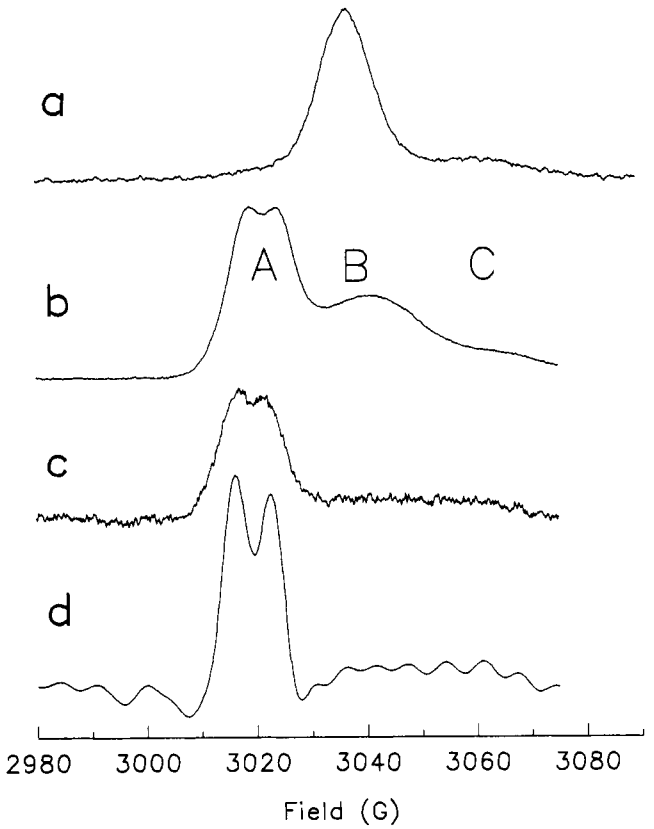

FIGURE 2: Comparison of $-5/2_{\parallel}$ features of the EPR signals that arise from VO^{2+} bound to CF_1 under various conditions. (a) Spectrum obtained under conditions listed in Figure 1a (1.5 ATP per VO^{2+}) except for SR, 5.3 G/s; and 16 scans. (b) Spectrum obtained under conditions of Figure 1b (3 ATP per VO^{2+}) except for SR, 4.8 G/s; TC, 41 ms; and 200 scans. (c) Spectrum of sample from spectrum b after extensive gel filtration chromatography as described in Experimental Procedures. Sample contained 0.375 mM CF_1. EPR conditions were the same as in b except for 9.5497 GHz and 50 scans. (d) Resolution enhancement of c using line width, 6.07 G, and L 0.011.

spectrum is what appears to be a doublet at 3020 G (feature A, Figure 2b). This represents a shift of the $-5/2_{\parallel}$ line to a lower field by about 20 G from feature B (Figure 2a), which arises from VO^{2+} bound in the absence of ATP. Feature C (Figure 2b) at about 3060 G is also present in relatively low abundance. The integrated areas of features A–C in Figure 2b were determined as described in Experimental Procedures. In the average of three experiments, where the mole ratio of CF_1:VO^{2+}:ATP was 1.5:1:3, relative integrated intensities of features A–C were 40, 40, and 20%, respectively.

Figure 2c shows the EPR spectrum of the bound VO^{2+} after the sample of Figure 2b was depleted of metal and nucleotide by extensive gel filtration chromatography, a treatment known to deplete nucleotides from all but the N1 and N2 sites. Though the signal-to-noise ratio was lower due to protein loss during the procedure, it is clear that the VO^{2+} that gives rise to feature A has not been removed. Incubation of this sample as an ammonium sulfate precipitate, a treatment that removes ATP from the N2 site, was required to remove the VO^{2+} bound to this site as determined by atomic absorption spectroscopy. These results imply that feature A results from a single species of bound VO^{2+} rather than two different species with overlapping spectra. Since this same treatment is required to deplete the enzyme of nucleotide from the N2 site, which then binds ATP in a strictly metal-dependent manner, this strongly suggests that feature A represents the metal bound in association with the ATP at the N2 site.

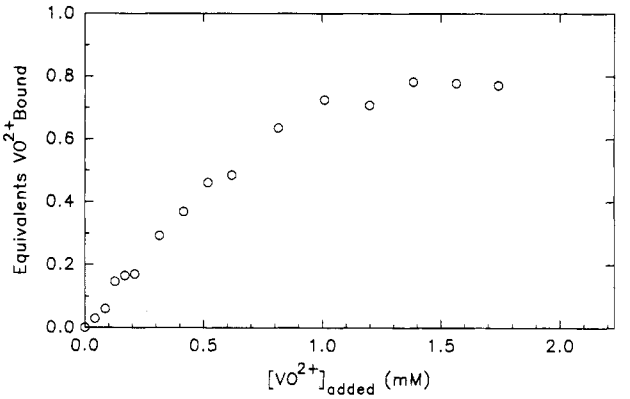

FIGURE 3: Extent of binding of VO^{2+} as a function of the VO^{2+} concentration added as a 3:1 ATP:VO^{2+} ratio to CF_1 to produce feature A. The sample contained 62 mg of CF_1 in 0.45 mL, and the amount of bound VO^{2+} was monitored by the integrated signal intensity of the $-5/2_{\parallel}$ signal that corresponded to feature A. Quantitation of the amount of bound VO^{2+} from the signal intensity was determined as per Houseman et al. (1994). EPR conditions were as in Figure 2b except for 32 scans and 82 ms TC. Calculation of K_D is not feasible because VO^{2+} is known to precipitate at high pH unless it is complexed to ligands in solution.

The titration curve of feature A shown in Figure 3 further supports the assignment of the two peaks composing feature A in spectra b and c of Figure 2 to a doublet that arises from a single bound VO^{2+}. Aliquots from a solution of ATP and VO^{2+} in the ratio of 3:1 were added to nucleotide-depleted CF_1 until no further increase in feature A was observed. Throughout the entire titration, the intensities of the two peaks in the doublet were equal (data not shown). The EPR intensity of feature A was integrated and correlated to the amount of bound VO^{2+} as described in Experimental Procedures. The plot of equivalents of bound VO^{2+} versus concentration of added VO^{2+} shows a hyperbolic curve that saturates at about one site. This result is consistent with the assignment of feature A to VO^{2+} bound at the single M2 site that fills in a manner analogous to the metal-dependent binding of ATP at the N2 site.

The doublet in feature A (Figure 2b,c) is characteristic of superhyperfine interaction with a ligand nucleus having A_{obs} = 6.6 G or 18 MHz as determined by resolution enhancement (Figure 2d). The doublet implies that the interacting nucleus has $I = 1/2$ and must, therefore, be either ^1H of ^{31}P. However, ^1H coupling to VO^{2+} is typically much smaller than 18 MHz on a parallel EPR line as shown by frozen-solution and single-crystal ENDOR (Böttcher et al., 1979; Kirste & van Willigen, 1982; Atherton & Shackleton, 1980). Thus, the doublet must result from the coordination of a phosphate oxygen with the metal. The 6.6 G splitting is seen on the $-5/2_{\parallel}$ EPR line, which represents only VO^{2+} complexes oriented with the V=O bond along the magnetic field and with the coordinated phosphate O—V bond lying nearly along a line perpendicular to the field. Hence, the observed splitting can be assigned to $A_{\perp}$ of ^{31}P. As shown in Table 1, the magnitude of this coupling is similar to that observed for ^{31}P from equatorially ligated phosphate of VO^{2+}–ATP complexes in solution (Mustafi et al., 1991) and bound to AdoMet synthetase (Markham, 1984). The fact that the coupling results in a doublet indicates that only one of the three phosphates of ATP is equatorially coordinated. The small hyperfine coupling expected from axially coordinated nuclei may prevent observation of any axially coordinated phosphate (see Discussion). These results show that feature A is the result of VO^{2+} and ATP bound to the M2 and N2 sites, respectively, forming an apparent monodentate M2–N2 complex.

Table 1: Experimentally Determined ^{31}P Hyperfine Couplings for VO^{2+} Complexes

VO^{2+} equatorial ligands	$^{31}P\ \lvert A_\perp \rvert$ (MHz)	ref
CF_1 + nucleotide		this paper
feature A	18.5	
feature B		
feature C	20	
AdoMet synthetase		*a*
$1RNH_2$ (K^b), $2P_i$ (ATP), $1H_2O$	21.4	
$1RNH_2$ (K^b), $2P_i$ (PPP_i), $1H_2O$	20.4	
$1RNH_2$ (AdoMet), RO^-? (S or T^b)	21.1	
2ATP:4P_i	18.5	*c*

[a] Zhang et al. (1993) and Markham (1984). [b] Refers to single-letter abbreviation of amino acid side chain. [c] Mustafi et al. (1991) reported $|A_\parallel|$; but for comparison, Zhang (1993) found $|A_\parallel|$ to be only ~3.4 MHz larger than $|A_\perp|$.

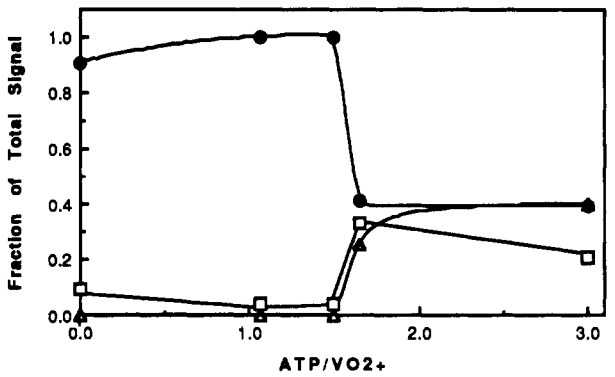

FIGURE 4: Fractional amounts of VO^{2+} bound to CF_1 in the forms that give rise to features A (△), B (●), and C (□) as a function of the ratio of ATP per VO^{2+} added. The fractional binding was determined by the integrated area under the $-5/2_\parallel$ features after the addition of 0.67 equiv of VO^{2+} to CF_1 at the ATP:VO^{2+} ratios indicated.

Dependence of VO^{2+} Binding Environment on the ATP:VO^{2+} Ratio. In Figure 4, the relative peak intensities of features A–C are plotted as a function of the ATP:VO^{2+} ratio upon addition of 0.67 mol of VO^{2+}/mol of CF_1. When no nucleotide is present in solution, the monodentate VO^{2+}-ATP complex cannot form, resulting in the formation of feature B alone. The abundance of feature B predominates even when ATP is added to the solution until the ATP:VO^{2+} ratio reaches 1.7:1.0 at which point features A and C appear at the expense of a proportional amount of feature B. It has not been possible, to date, to bind VO^{2+} to CF_1 in a manner that produces feature A without also yielding a significant amount of feature B. These results suggest that the formation of features A and C is due to changes in the ligands of the bound VO^{2+}, particularly the coordination of ATP to the metal, rather than to the appearance of new VO^{2+} binding sites at different locations from those that give rise to feature B. Consequently, at low ATP:VO^{2+} ratios, feature B represents VO^{2+} bound at the M2 and M3 sites. At high ratios, the single site represented by feature A is VO^{2+} bound in the M2–N2 form and suggests that the residual feature B (and perhaps also feature C) represents the VO^{2+} bound at the M3 site.

When ATP binding was measured directly using [2,8-^{3}H]-ATP for Mg^{2+} and VO^{2+} at both 3:1 and 1.5:1 ATP:M^{2+} ratios, it was found that ATP bound at N2 to the same degree at both ratios of ATP:M^{2+} for both metals (data not shown). This result shows that the amount of ATP bound to N2 is independent of the type of metal and the ATP:M^{2+} ratio, provided that metal is present. The ratio of ATP:VO^{2+} only affects whether ATP at the N2 site is coordinated to the metal at the M2 site.

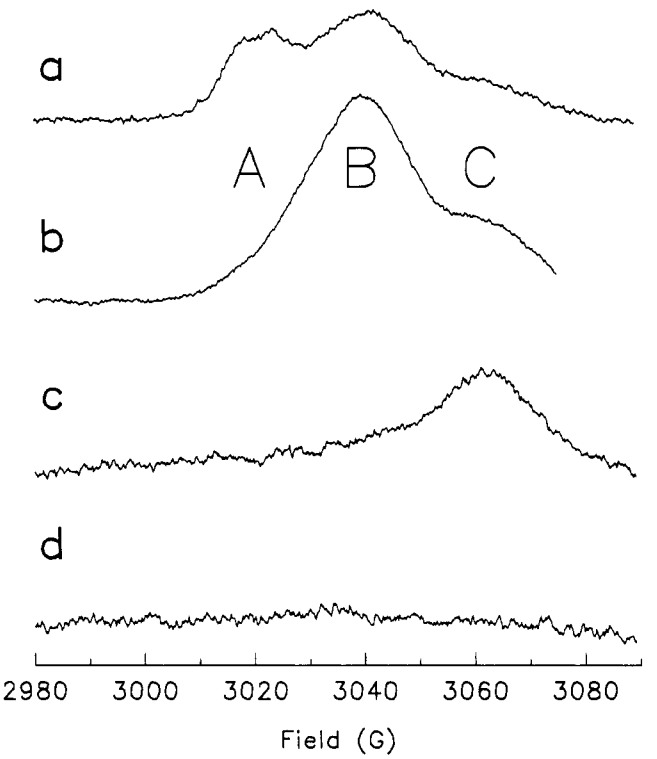

FIGURE 5: Comparison of $-5/2_\parallel$ features of the EPR signals that arise from VO^{2+} bound to the M3 or M2 and M3 sites of CF_1 under various conditions. (a) Latent CF_1 after the addition of excess 3 ATP per VO^{2+} followed by gel filtration chromatography and the addition of ADP and VO^{2+} to CF_1 in a ratio of 1:1:1. (b) Latent CF_1 with excess 2 ATP per Mg^{2+} added to fill M2–N2 followed by chromatography and the addition of ADP and VO^{2+} to CF_1 in the ratio of 1:1:1 to fill M3 and N3. (c) Sample from b after activation of CF_1 with 50 mM DTT and 20% ethanol. (d) Sample from c after gel filtration chromatography. EPR conditions were as in Figure 3a except (a) 9.5525, (b) 9.5555, (c) 9.5524, and (d) 9.5529 GHz and (a) 32, (b) 100, (c) 256, and (d) 128 scans.

Binding of VO^{2+} to the M3 Site. To examine the M3 binding site with VO^{2+}, samples were prepared in a two-step process. In the first step, the M2–N2 site was filled with VO^{2+}–ATP as per Figure 2b and chromatographed to remove metal–nucleotide from binding sites with lower affinity under conditions as per Figure 2c so that only feature A was present. In the second step, VO^{2+} was added with ADP to fill the M3 and N3 binding sites of latent CF_1. Figure 5a shows the $-5/2_\parallel$ line of the VO^{2+} bound to CF_1 under these conditions. Two new features were observed that closely resembled features B (3040 G) and C (3060 G). The appearance of these new signals did not alter the intensity or line width of feature A significantly.

The samples of Figure 5b,c were prepared in the same two-step manner as the sample of Figure 5a, but M2–N2 contained Mg^{2+}–ATP while M3 and N3 contained VO^{2+} and ADP. The use of ADP to fill the N3 site ensured that the VO^{2+}–ADP complex would not enter the N2 site (Bruist & Hammes, 1981). When prepared under these conditions, the latent enzyme (spectrum b) gives rise only to features B and C with the feature B-like form predominant. Feature A was absent because the M2–N2 site had been preloaded with Mg^{2+}–ATP.

Activation of the ATPase activity in the sample that gives rise to spectrum b by the addition of 50 mM DTT and 20% ethanol results in spectrum c. Within 5 min, this activation induces a change in the relative abundance of the two forms of the VO^{2+} bound to the M3 site such that feature C in Figure 5c is present almost exclusively. Very little change in

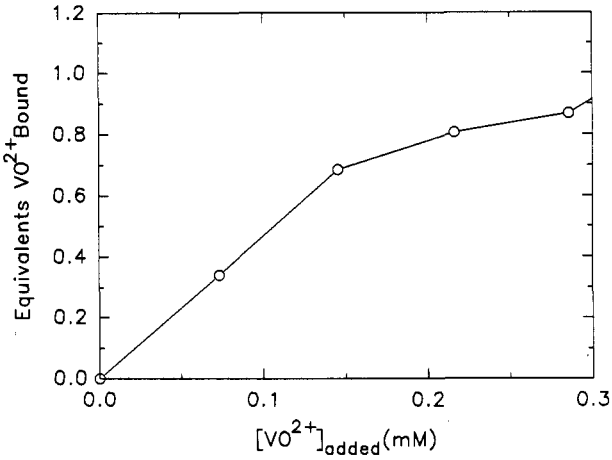

FIGURE 6: Titration of M3 with VO^{2+}–ADP. CF_1 was activated and stripped of metal–nucleotide by gel filtration chromatography. The final concentration of CF_1 was 61.4 mg/mL. A ratio of 3:1 ADP:VO^{2+} was used in titration, and the extent of binding to M3 was determined by monitoring feature C of the $-5/2_{\parallel}$ region of the EPR signal.

the spectrum occurs after further incubation for 15 min, and no change is apparent after a third 15-min incubation period. Filling the M3 and N3 sites with VO^{2+} and ATP also resulted in feature B in the latent enzyme that was converted to feature C upon activation (data not shown), suggesting nearly identical ligands to VO^{2+} in the two cases.

When CF_1 was omitted from a control sample containing the same amounts of VO^{2+}, ATP, DTT, and ethanol, a complex of VO^{2+} and DTT produced a feature at a higher field (~3070 G) in the $-5/2_{\parallel}$ region of the EPR spectrum with one-third the intensity of feature C (~3060 G). In contrast to VO^{2+} bound to CF_1, the remaining VO^{2+} in the control sample is present as EPR-silent species (Chasteen, 1981). This indicates that DTT has a lower affinity for VO^{2+} than does CF_1 such that it is unlikely that DTT can deplete the VO^{2+} from M3 in CF_1 (feature B). From these observations as well as the fact that feature C is present in the absence of DTT, it is clear that feature C arises from VO^{2+} bound to CF_1 and not from a VO^{2+}–DTT complex. Thus, activation of the enzyme induces the conversion of VO^{2+} bound at the M3 site from the feature B form to the feature C form.

Gel filtration chromatography is sufficient to remove ADP bound to the N3 site (Bruist & Hammes, 1981). As shown in Figure 5d, a comparable chromatography treatment depletes the VO^{2+} bound to the M3 site that gave rise to feature C from CF_1. In samples of CF_1 containing VO^{2+} that result in feature A (Figure 2c), this same chromatography treatment not only abolishes feature C but also abolishes feature B. These results show that the conditions that deplete nucleotide from the N3 site also remove the VO^{2+} bound at the M3 site in either the feature B or feature C forms.

Titration of the M3 site in activated CF_1 is shown in Figure 6 using a 3:1 ADP:VO^{2+} ratio. CF_1 was prepared as in Figure 5b, but was activated before the addition of metal and nucleotide. The use of ADP ensured that no metal–nucleotide complex could form at the M2–N2 site (Bruist & Hammes, 1981). The abundance of bound VO^{2+} that gave rise to feature C, determined as described in Experimental Procedures, saturated at about one site.

DISCUSSION

Four different VO^{2+} binding environments have now been discerned on CF_1 that correspond to feature A, feature C, and two feature B types of the $-5/2_{\parallel}$ line of the VO^{2+} EPR signal. We conclude that the VO^{2+} binding site that gives rise to feature A results from a monodentate metal–nucleotide complex bound to the noncatalytic N2 nucleotide-binding site based on the observation that the $-5/2_{\parallel}$ line is a doublet with a coupling of 6.6 G (Figure 2c). As shown in Table 1, the observed ^{31}P coupling is consistent with other observations of equatorial phosphate coordination to VO^{2+}. These couplings are relatively small considering the large magnetic moment of the ^{31}P nucleus. The observed superhyperfine coupling to ligands of VO^{2+} is much smaller than that of Cu^{2+} where the unpaired electron resides in the $d_{x^2-y^2}$ orbital which points directly at the ligands (Brown & Hoffman, 1980). For example, the coordinated ^{14}N nuclei of the porphyrin ligand in Cu^{II}(tetraphenylporphyrin) have an isotropic superhyperfine coupling of $|A| = 47$ MHz, whereas the ^{14}N coupling in $V^{IV}O$(octaethylporphyrin) is only $|A| = 7.2$ MHz (Fukui et al., 1993). Since even less spin density can be transferred to an axial ligand of VO^{2+}, the magnitude of the observed superhyperfine coupling suggests equatorial ligation.

The monodentate metal–ATP complex must be bound to the noncatalytic N2 site based on the observations that (i) binding of ATP to the N2 site is strictly metal dependent (Bruist & Hammes, 1981; Shapiro et al., 1991); (ii) although the protein does contain ADP bound to N1, the addition of VO^{2+} in the absence of nucleotide does not give rise to feature A, only feature B for which no ^{31}P coupling is evident, and we have observed feature A when the depleted enzyme still contained Mg^{2+} at the M1 site; (iii) the VO^{2+} bound to CF_1 that gives rise to feature A is not depleted by extensive gel filtration chromatography but requires ammonium sulfate precipitation of the protein as required for the removal of ATP from the N2 site (Bruist & Hammes, 1981); and (iv) the monodentate complex bound to this site is clearly different from the tridentate metal–ATP complex that exists at the catalytic sites of the activated enzyme (Frasch & Selman, 1982).

The evidence presented here suggests that the VO^{2+} bound to the M2 site can give rise to feature A as well as feature B. In the absence of added ATP, the bound VO^{2+} only gives rise to feature B (Houseman et al., 1994). However, it was noted that this filled both M2 and M3 sites. The same single feature occurs in the presence of ATP until the concentration of ATP approaches twice the concentration of VO^{2+}. Feature A then appears at the expense of the intensity of feature B. Apparently, the conversion of the M2 site to the M2–N2 site requires the binding of ATP to a separate site.

The conversion from feature B to feature A was observed to occur over a very narrow range of ATP:VO^{2+} ratios in Figure 4. This is likely to be the result of tight VO^{2+}–ATP coordination in solution. In fact, maximal stabilization of VO^{2+} is achieved under these conditions by chelation with two ATP molecules (Mustafi et al., 1992) so that significant noncoordinated ATP would not appear in solution until a nucleotide:metal ratio of approximately 2:1 was attained as is observed in Figure 4. Although the VO^{2+}–$(ATP)_2$ complex is present in solution at all ATP:VO^{2+} ratios above zero, its presence does not produce feature A. If the VO^{2+}–$(ATP)_2$ complex were responsible for the formation of feature A directly, minimally a 1:2:1 triplet would be observed, and the field position of feature A would be shifted to a higher field as per the additivity relation (Chasteen, 1981; Houseman et al., 1994). Rather, only as the ATP:VO^{2+} ratio approaches 2:1 will a significant concentration of free ATP exist in solution. Thus, the presence of free ATP is the likely cause of the

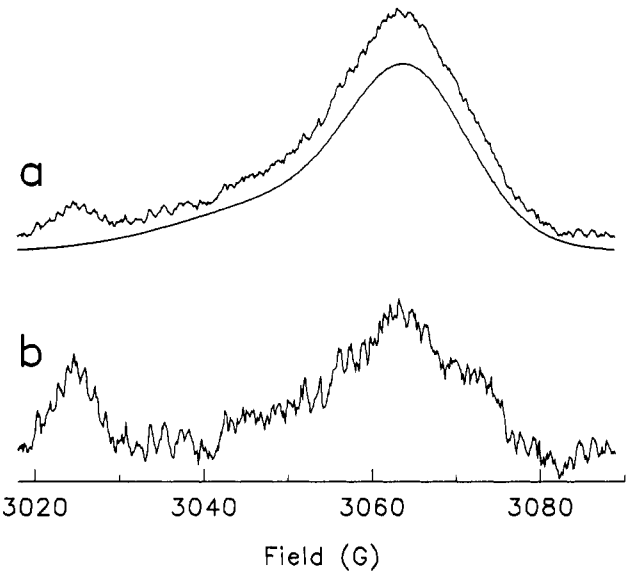

FIGURE 7: Resolution of 1:2:1 triplet from ^{31}P of bidentate ATP in feature C. (a) Experimental spectrum of activated CF_1 (88 mg/mL) preloaded with VO^{2+}–ATP in a 3:1 ATP:VO^{2+} ratio. EPR conditions same as in Figure 1a except 9.5532 GHz; (SR), 5.4 G/s; 1024 scans. (Inset to a) Two Gaussians fit to feature C and the small amount of remaining feature B using SpectraCalc. (b) Difference of a and 0.8× (inset).

transition in Figure 4. Because of this preferred VO^{2+}–ATP stoichiometry, however, such a change from metal to metal–nucleotide binding with Mg^{2+} would probably occur over a broader concentration range and at a different ratio.

A very close interaction between the M2 and N2 sites is also indicated by ATP- and M^{2+}-depletion experiments. Removal of ATP from the N2 site is necessarily a two-step process involving incubation as an ammonium sulfate precipitate in EDTA followed by extensive gel filtration chromatography (Bruist & Hammes, 1981). We have found that the first step is sufficient to deplete CF_1 of the metal bound to the M2 site. This and the fact that the N2 site requires metal to bind ATP suggest that the metal must be removed from M2 before the N2 site can be depleted of ATP.

Despite the dependence of nucleotide binding at N2 on the presence of metal and the dependence of VO^{2+}–ATP coordination at M2–N2 on the ATP:M^{2+} ratio, this ratio is not important for the binding of ATP to N2. At low ATP:VO^{2+} ratios, and hence low free ATP concentration, both ATP and VO^{2+} can still bind to the N2 and M2 sites separately. However, a direct link between the metal and the nucleotide is formed only when free ATP is available to bind to another nucleotide-binding site.

The fraction of feature B that remains under conditions where the intensity of feature A is maximal represents the population of VO^{2+} in the M3 site. This is indicated by the ability of gel filtration chromatography to remove the VO^{2+} corresponding to feature B but not that corresponding to feature A, which titrates to a single site. Due to the ability of gel filtration chromatography to deplete selectively the M3 binding site (Figure 2b,c) verification that this was the M3 site was obtained by selectively filling M3 with VO^{2+}, which gave rise to feature B (Figure 5a,b). The observation that activation of CF_1 converts all of the VO^{2+} bound at M3 into a form that gives rise to feature C, which is also removed by chromatography (Figure 5c,d), strongly suggests that the M3 binding site also exists in two forms.

Evidence supports the N3 site as a catalytic site (Bruist & Hammes, 1981). The nucleotide phosphates at these sites

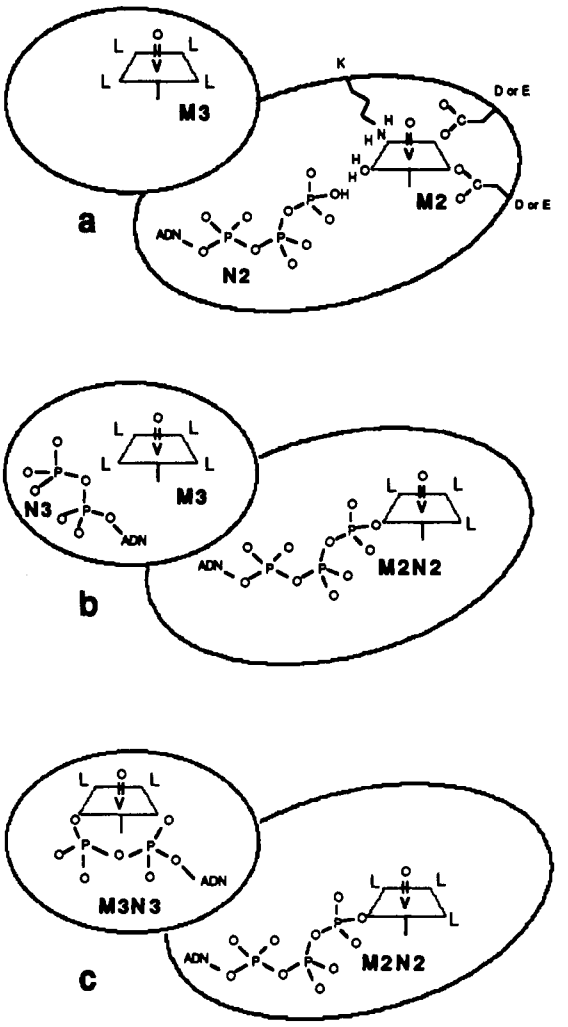

FIGURE 8: Summary of metal coordination at the M2 and M3 sites. L refers to unidentified ligands. (a) Addition of VO^{2+} to latent CF_1 such that no free ATP is present. (b) Addition of VO^{2+} to latent CF_1 such that free ATP is present. (c) Addition of VO^{2+}–ADP to metal- and nucleotide-depleted activated CF_1.

are coordinated to metal in the activated form (Frasch & Selman, 1982; Carmeli et al., 1989; Devlin, & Grisham, 1990), but not in latent CF_1 (Carmeli et al., 1989). Unlike the M2–N2 site, the ^{31}P couplings in feature C are not clearly resolved. From the stereochemistry of the catalytic site (Frasch & Selman, 1982), a 1:2:1 triplet is predicted for the bidentate ADP–VO^{2+} complex and either a quartet or triplet for the VO^{2+}–ATP complex at M3–N3 depending on whether an equatorial or facial tridentate complex, respectively, is formed. In facial tridentate coordination, only two cis, equatorial positions are occupied, leading to a 1:2:1 triplet, but the third ligand is at the weak, axial position, so its hyperfine splitting is not likely to be resolved in the EPR spectrum. If the coupling is about 6.6 G as observed for the M2–N2 site, the expected resolution of ^{31}P coupling is no more than that observed for feature C.

Figure 7 shows a means of determining whether ^{31}P couplings are present in feature C arising from ADP–VO^{2+} bound to M3–N3. SpectraCalc was used to obtain the best fit of feature B and feature C to Gaussian line shapes (Figure 7a). Subtraction of 80% of this fit from the experimental spectrum (spectrum b) showed that the residual intensity of feature B was Gaussian, but that the residual intensity of feature C was a triplet. A ^{31}P coupling of about 7 G or 20 MHz was obtained, which is within the reported range shown in Table 1. The intrinsic line width appears to be larger in

this triplet than in the doublet of Figure 2d, probably due to additional unresolved hyperfine coupling from the presence of more protons in the M3–N3 site than in the M2–N2 site. However, due to the uncertainty of this technique, confirmation that feature C results from the M3–N3 metal–nucleotide complex must await experiments that employ ^{17}O-labeled nucleotides.

In summary, the data presented here suggest that, when little free ATP is available to bind independently of metal, the metal binds in a cooperative manner to the M2 and M3 sites (Houseman et al., 1994). Although the nucleotide can bind to the N2 site at this time, it is not coordinated to the metal (Figure 8a). Binding of a nucleotide to a separate site induces the M2 site to become the M2–N2 site (Figure 8b). This separate site is possibly the N3 site, although other sites with lower affinity cannot be ruled out. In the latent form of the enzyme a nucleotide that binds to N3 under these conditions is also not coordinated to the metal at M3, but activation of the ATPase activity induces formation of a metal–nucleotide complex at the M3–N3 site (Figure 8c).

ACKNOWLEDGMENT

The authors thank Allyson Roskelley and Alexander Gray for technical support.

REFERENCES

Atherton, N. M., & Shackleton, J. F. (1980) *Mol. Phys. 39*, 1471–1485.
Böttcher, R., Heinhold, D., & Windsch, W. (1979) *Chem. Phys. Lett. 65*, 452–455.
Brown, T. G., & Hoffman, B. M. (1980) *Mol. Phys. 39*, 1073–1109.
Bruist, M. F., & Hammes, G. G. (1981) *Biochemistry 20*, 6298–6305.
Carmeli, C., Huang, J., Mills, D., Jagendorf, A., & Lewis, A. (1986) *J. Biol. Chem. 261*, 14171–14177.
Carmeli, C., Lewis, A., & Jagendorf, A. T. (1989) in *Current Research in Photosynthesis* (Baltscheffsky, M., Ed.) Vol. III, pp 29–32, Kluwer, Dordrecht.
Chasteen, N. D. (1981) in *Biological Magnetic Resonance* (Berliner, L., & Reuben, J., Eds.) pp 53–119, Plenum Press, New York.
Devlin, C., & Grisham, C. (1990) *Biochemistry 29*, 6192–6203.
Frasch, W. D. (1994) in *The Molecular Biology of Cyanobacteria* (Bryant, D. A., Ed.) Kluwer Academic Publishers, The Netherlands (in press).
Frasch, W. D., & Selman, B. R. (1982) *Biochemistry 21*, 3636–3643.
Fukui, K., Ohya-Nishiguchi, H., & Kamada, H. (1993) *J. Phys. Chem. 97*, 11858–11860.
Haddy, A. E., Frasch, W. D., & Sharp, R. R. (1985) *Biochemistry 24*, 7926–7930.
Hiller, R., & Carmeli, C. (1985) *J. Biol. Chem. 260*, 1614–1617.
Hochman, Y., & Carmeli, C. (1981) *Biochemistry 20*, 6287–6292.
Houseman, A. L. P., Morgan, L., LoBrutto, R., & Frasch, W. (1994) *Biochemistry 33*, 4910–4917.
Kauppinen, J. K., Moffat, D. J., Mantsch, H. H., & Cameron, D. G. (1981) *Appl. Spectrosc. 35*, 271–276.
Kirste, B., & van Willigen, H. (1982) *J. Phys. Chem. 86*, 2743–2749.
Latwesen, D. G., Poe, M., Leigh, J. S., & Reed, G. H. (1992) *Biochemistry 31*, 4946–4950.
Leckband, D., & Hammes, G. G. (1987) *Biochemistry 26*, 2306–2312.
Markham, G. D. (1984) *Biochemistry 23*, 471–478.
Murataliev, M. B. (1992) *Biochemistry 31*, 12885–12892.
Mustafi, D., Telser, J., & Makinen, M. W. (1992) *J. Am. Chem. Soc. 114*, 6219–6226.
Senior, A. E., & Al-Shawi, M. K. (1992) *J. Biol. Chem. 267*, 21471–21478.
Shapiro, A. B., Huber, A. H., & McCarty, R. E. (1991) *J. Biol. Chem. 266*, 4194–4200.
Zhang, C. (1993) Ph.D. Dissertation, Northeastern University, Boston, MA.
Zhang, C., Markham, G. D., & LoBrutto, R. (1993) *Biochemistry 32*, 9866–9873.